PAPER

The impact of doped silicon quantum dots on human osteoblasts

Lucie Ostrovska,[ab] Antonin Broz,[bc] Anna Fucikova,[d] Tereza Belinova,[e] Hiroshi Sugimoto,[f] Takashi Kanno,[f] Minoru Fujii,[f] Jan Valenta[d] and Marie Hubalek Kalbacova[*ab]

Silicon (Si) nanostructures allow for the expansion of the application spectrum of this important semiconductor material with respect to the fields of optoelectronics and photonics. At the same time, the significant potential of Si quantum dots (SiQDs) has been revealed in terms of their potential application in the areas of biology and medicine due to their biocompatibility, low toxicity and natural biodegradability, unlike currently used semiconductor quantum dots. As far as this study is concerned, SiQDs co-doped with boron and phosphorus were used for the *in vitro* evaluation of their cytotoxicity in human osteoblasts. Two chemically identical types of SiQD differing in terms of their size and photoluminescence (PL) were studied. They both display long-lasting dispersion in methanol and even in aqueous media as well as PL which is not sensitive either to changes in the environment or surface modifications. Our experiments revealed significant differences between the two types of SiQD tested in regard to their behavior in a cell culture environment depending on increasing concentration (25–125 μg ml^{-1}) and cultivation conditions (the presence or absence of proteins from the fetal bovine serum – a component of the cultivation medium). A detailed description of their optical parameters and the evaluation of zeta potential enhance the understanding of the complexities of the *in vitro* results obtained.

1 Introduction

Various types of nanoparticles have been studied and used in different fields of science including their application in the field of bio-medicine. In general, nanoparticles (so-called quantum dots – QD) based on a variety of materials provide a promising tool with regard to potential as drug and gene carriers and as imaging and diagnostic platforms.

Silicon-based nanoparticles make up one of the most promising platforms yet determined for medicinal application due to their high level of biocompatibility and biodegradability which arise from the fact that silicon (Si) is an essential trace element in the human body. Currently, the development of various types of Si-based nanoparticles is focused principally on silica (SiO$_2$) and pure silicon materials which are biodegradable

due to the nature of their Si–Si and Si–O bonds.[1,2] In addition, it is essential to note that most Si-based nanoparticles possess the quality of fluorescence (photoluminescence) and therefore facilitate their own imaging without any additional intervention into their structure being required.[3,4] Moreover, their dispersibility in aqueous solutions is also crucial for bio-application.[5] Such properties are similar to the afore-mentioned QDs, thus the term silicon quantum dots (SiQD) is particularly appropriate.

This study is concerned particularly with the assessment of cytotoxicity since this makes up the most important initial step preceding the actual application of any of the materials studied in terms of human medicine. Previous studies have shown that the cytotoxicity of Si-based nanoparticles is influenced by a range of properties such as particle shape, size, zeta potential, dose and chemical composition[6–12] and some of these properties may play a role in the formation of so-called biomolecular coronas. This term describes a layer of biomolecules, mainly proteins (protein corona), originating from the biological environment surrounding nanoparticles which accord them a new identity which differs from that of bare nanoparticle in terms of a number of characteristics especially their reaction with organisms.[13,14] Generally, the concept of the protein corona is given as a biological identity *via* which nanoparticles are presented to cells. It has been suggested that the presence, and possibly the composition, of the protein corona provides the key

[a]*Biomedical Center, Faculty of Medicine in Pilsen, Charles University in Prague, Pilsen, Czech Republic. E-mail: marie.kalbacova@lf1.cuni.cz*

[b]*Institute of Inherited Metabolic Disorders, 1st Faculty of Medicine, Charles University in Prague, Prague, Czech Republic*

[c]*Institute of Physiology, Academy of Sciences of the Czech Republic, Prague-Krč, Czech Republic*

[d]*Faculty of Mathematics and Physics, Prague, Czech Republic*

[e]*Department of the Cell Biology, Faculty of Science, Charles University in Prague, Prague, Czech Republic*

[f]*Department of Electrical and Electronic Engineering, Graduate School of Engineering, Kobe, Japan*

to the determination of the cytotoxicity of nanoparticles.[15,16] *In vivo*, the composition of the attached proteins is spatial (lung fluids, bloodstream) and time dependent and, moreover, the condition of the living organism should be considered.[16] On the other hand, *in vitro* conditions are limited by the presence of certain types of proteins contained within the selected supplemented serum; thus, it appears that the protein corona is not subject to the same degree of significant dynamic change in composition as it is *in vivo*.[17]

Previous studies that have focused on the impact of silica nanoparticles (SiO$_2$ NPs) on keratinocytes revealed that the viability of cells is both dose- and size-dependent and, in addition, that this particular type of particle causes damage to the cellular membrane which may be of either chemical or mechanical stress origin.[7,8] It has been proposed that cytotoxicity caused by SiO$_2$ NPs may be the result of oxidative stress induced by the production of intracellular reactive oxygen species.[11,18] However, when compared to other types of nanoparticles, *e.g.* ZnO particles, SiO$_2$ NPs reveal lower cytotoxicity levels dependent on the cell type.[7,9,19] Moreover, a number of papers has reported a significant correlation between cytotoxicity and the dose of Si-based nanoparticles (irrespective of the actual concentration range used for a particular cellular type). Generally, the higher the nanoparticle dose applied to the cells, the higher is the cytotoxicity observed following a certain period of time, an example of which is provided by studies by Bhattacharjee *et al.* wherein increasing concentrations from 0.1 ng ml^{-1} to 100 μg ml^{-1} of nanoparticles were added to a cell culture of NR8383 macrophages. The same cytotoxicity trend was also evident with respect to keratinocytes, although the concentrations applied were significantly higher (25–500 μg ml^{-1}).[8,10,11] It is possible to obtain a better understanding of the causes of the cytotoxicity of particular nanoparticles by means of a description of specific cell–nanoparticle interactions.

It is widely accepted that nanoparticles of different types enter cells by means of endocytosis, *i.e.* a form of active transport; however, the specific ways in which individual particles enter certain cell types remain to be discovered. Considerable interest has been devoted to the discovery of principal nanoparticle uptake pathways and most of the experiments conducted in this respect were performed *via* the selective gradual blocking of different pathways and the subsequent determination of which was most frequently used. Clathrin- and caveolin-dependent endocytotic pathways have been suggested as the main routes used by silicon-based particles; however, a number of studies also suggest the use of the flotillin-dependent pathway.[12,20] It has been implied that the principal pathway is determined not only by particle size and shape but also by cellular type. It is important to gain an understanding of all the interactions which take place between cells and nanoparticles so as to avoid any harmful effects in terms of potential use in human medicine.

This study employed two types of SiQD of different characteristics (SiQD 1050 – 3 nm size, 750 nm peak emission and SiQD 1100 – 4 nm size, 850 nm peak emission) and their influence on a biological system represented by a human osteoblast-like cell line (SAOS-2) was compared. The main focus

of the study was (i) to determine the appropriate concentration of both types of SiQD based on the induced cytotoxicity and (ii) to evaluate the cellular uptake of both SiQDs at 2, 6 and 24 hours by means of fluorescence wide-field and confocal microscopy. The influence of the presence of fetal bovine serum (FBS) in the cultivation media made up an important variable parameter in terms of understanding the impact of the protein corona on SiQD behavior *in vitro*.

2 Experimental

2.1 The fabrication of co-doped SiQDs

P and B co-doped colloidal Si QDs were synthesized by means of a previously reported procedure.[21,22] Si-rich borophosphosilicate (BPSG) films were deposited on thin stainless steel plates *via* the co-sputtering of Si, SiO$_2$, B$_2$O$_3$, and P$_2$O$_5$ using the rf-sputtering apparatus. The films were then peeled from the plates and crushed to powder form in a mortar. The powder was then annealed at different temperatures (1050 °C and 1100 °C thus obtaining SiQD 1050 and SiQD 1100 respectively) in an N$_2$ gas atmosphere for 30 minutes so as to cultivate SiQDs of differing size in BPSG matrices. During the growth of the SiQDs, P and B atoms were incorporated into Si–NCs from the BPSG matrices.

2.2 The detailed optical characterization of co-doped Si-QD

Transmission electron microscopy images were obtained using JEOL JEM-200CX, and the IR absorbance of the suspensions measured by means of drop-casting on a gold covered silicon substrate in an FT-IR spectrometer (Perking Elmer, Spectrum GX). UV-VIS spectra were measured by UV-3101PC (Shimadzu). The PL spectra (Fig. 1d) were obtained using a spectrofluorometer (Fluorolog-3, Horiba Jobin-Yvon).

The photoluminescence external quantum yield (EQY) of the SiQD suspensions was measured in specially-designed equipment based on an integrating sphere.[23] Excitation wavelengths were tuned over a broad spectral range from UV to yellow using either a set of light-emitting diodes or a white-light emitting laser-driven light source (LDLS, Energetiq) coupled to a 15 cm monochromator. The absorption cross-section σ was obtained by means of the intensity-dependent PL-modulation technique applied to a thin liquid layer of SiQD in methanol.[24] Under 405 nm excitation and an emission between 700 and 900 nm, σ was determined at around 3×10^{-16} cm^2 for both of the samples studied.

The PL kinetics of SiQDs under high-repetition short pulses (simulating the conditions of a confocal microscope with a "white" fiber laser) were tested for SiQD 1050 in a cuvette excited *via* a pulsed diode laser at 408 nm (pulse duration below 0.1 ns, 20 MHz repetition rate and 840 W cm^{-2} power density) (Fig. 3b).

2.3 Zeta-potential assessment

ζ was measured using a Malvern Zetasizer Nano ZS equiped with MPT-2 titration unit where 0.25 M NaOH, 0.2 M HCl and 0.02 HCl were used as titration agents. The SiQD suspensions were titrated in the acid to base and base to acid direction.
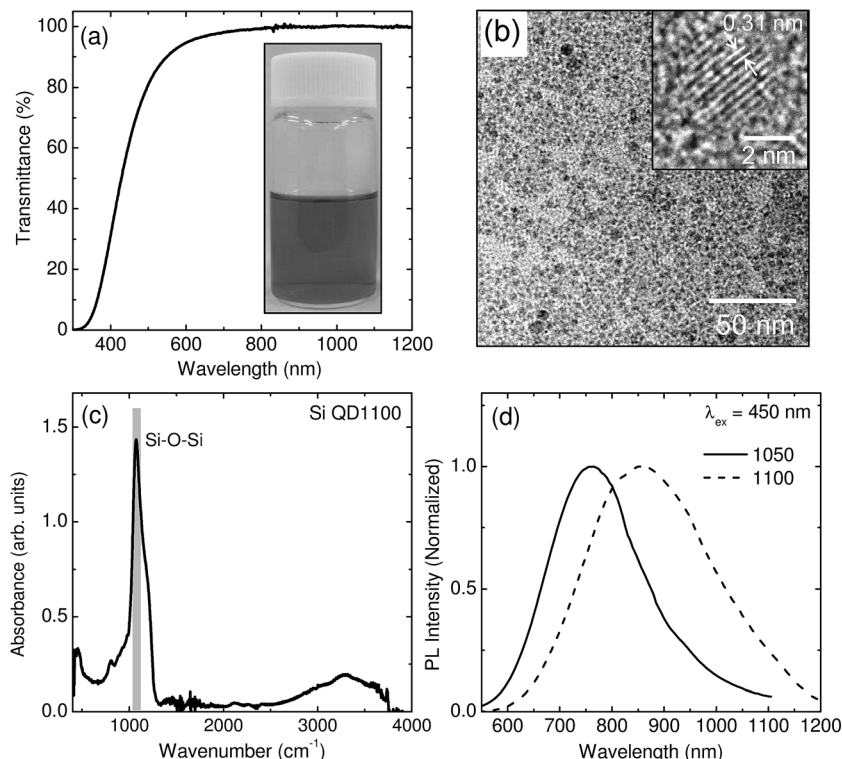
Fig. 1 (a) Optical transmittance spectrum and photograph of colloidal dispersion (methanol) of SiQD 1100; (b) TEM image of SiQD 1100, inset: high-resolution TEM image of a QD with lattice fringes corresponding to {111} plane of Si crystals; (c) IR absorption spectrum of SiQD 1100; (d) PL spectra of SiQD 1050 and 1100 (d).

2.4 Cell cultivation with SiQDs

SAOS-2 cells (DSMZ, Germany) were cultured in McCoy's 5A medium without phenol red (HyClone) and supplemented with 10 000 U ml^{-1} penicillin (Sigma-Aldrich) and 10 µg ml^{-1} streptomycin (Sigma-Aldrich) and, in some of the experiments, with 15% fetal bovine serum (Biosera). The cells were seeded at a density of 10 000 cells per cm^2 onto a 96-well plate (Techno Plastic Products) in triplets for the measurement of cytotoxicity (100 µl) or onto cell imaging dishes with a 145 µm glass bottom in singlets (Eppendorf) for microscopy purposes (500 µl). The cells were cultured for 24 hours in a humidified 5% CO$_2$ atmosphere at 37 °C.

The required amount of SiQD colloid in pure methanol was added to an equal amount of distilled water and the resulting mixture was subsequently incubated in a dry bath incubator (Major Science) set to 70 °C until half of the liquid had evaporated. The final SiQD colloid was ready for immediate dilution into the appropriate cultivation media. Two types of cultivation media were used in the experiments – McCoy's 5A medium without phenol red (HyClone) with 10 000 U ml^{-1} penicillin (Sigma-Aldrich) and 10 µg ml^{-1} streptomycin (Sigma-Aldrich) with no serum proteins (serum-free) or supplemented with 5% fetal bovine serum (Biosera) (serum-supplemented). The final concentrations of SiQD in the media used for cell treatment consisted of 125 µg ml^{-1}, 50 µg ml^{-1} and 25 µg ml^{-1}.

The cells were gently rinsed with phosphate buffer saline (PBS) prior to the addition of the cultivation media containing SiQDs. Subsequently, the cells were cultivated to different time points depending on the type of assessment. In the case of the serum-free media, an additional volume of 50 µl (96-well plate) or 250 µl (cell imaging dish) of the medium with 5% FBS was added after 6 hours of cultivation and cultivated for an additional 18 hours or 42 hours (in the case of 24 hours or 48 hours of cultivation time respectively).

2.5 Cytotoxicity assessment

The cytotoxicity of various concentrations of SiQDs in different media was assessed by means of the measurement of the metabolic activity of the cells at 6, 24 and 48 hours following the addition of SiQDs to the cells. Assessment was performed by means of MTS assay (Cell Titer96® AqueousOne, Promega). The principle of this colorimetric assay consists of the reduction of an MTS ((3-(4,5-dimethylthiazol-2-yl)-5-(3-carboxymethoxyphenyl)-2-(4-sulfophenyl)-2H-tetrazolium)) compound into a soluble colored formazan product via mitochondrial dehydrogenases. The assay was performed according to the manufacturer's instructions. The cells were rinsed three times with PBS and then incubated for 2 hours with an MTS reagent diluted in the appropriate media. Optical density was measured using a microplate reader (Synergy H1, BioTek) at 490 nm subtracting the background at 655 nm. The subtraction of blank values was conducted for each type of medium separately. All the results obtained were compared to the results of the control cells cultivated in a medium supplemented with 5% FBS; the results were expressed as percentages.

2.6 Fluorescence wide-field and confocal microscopy

After 2, 6 and 24 hours the cells were rinsed three times with PBS so as to remove any un-internalized SiQDs and then fixed in 4% paraformaldehyde. An Eclipse Ti–S epi-fluorescence microscope (Nikon) with Mercury Arc Lamp Intensilight HGF1 and equipped with DS-Qi1Mc digital camera (Nikon) was used in order to acquire 2D fluorescence images of SiQDs at an excitation wavelength of 330–380 nm and emission wavelength of 510–590 nm. The extent of the penetration of SiQDs in the *z*-axis of the cells was analyzed with respect solely to the 24 hour samples by means of a Leica TCS SP8X confocal laser scanning microscope (Leica Microsystems). The SiQDs were excited using a pulse continuum white light laser (475–499 nm, 80 MHz) and emissions were collected *via* a hybrid detector at 700–795 nm. The elimination of cell autofluorescence from SiQD signals was achieved by the gating of signal detection with a 5 ns delay from the excitation pulse while maintaining a detection width of 7 ns. Multiple line accumulation scanning and prolonged pixel dwell were set so as to allow for the more intense and precise imaging of the SiQDs. All the confocal 3D images were acquired by means of a Leica DFC365 FX monochrome digital CCD camera and further analyzed using LAS X core software (Leica Microsystems). The confocal images were processed using Hyugens software for deconvolution and maximum intensity projection. ImageJ software was subsequently used for contrast and smoothness correction purposes.

2.7 Statistical analysis

All the data presented was derived from three independent experiments performed in triplicate. The results are presented in the form of mean values with error bars indicating standard deviations. Data distribution was evaluated using the Shapiro–Wilk test. The nonparametric Wilcoxon matched pairs test was used in order to determine significant differences between the datasets and the control with 5% FBS and the rest of the variables. An ANOVA was used to compare differing SiQD concentrations at certain time points with each other. *p* values of less than 0.05 were considered statistically significant. Extreme values were excluded from the analysis. Statistical analysis was performed using STATISTICA (StatSoft, Inc.) software.

3 Results and discussion

3.1 The optical characterization of co-doped SiQD

Phosphorus (P) and boron (B) co-doped colloidal SiQDs were synthesized by means of a previously reported procedure.[21,22] The transmittance spectrum and an image of the colloid are shown in Fig. 1a. Transmittance around the band gap of bulk Si crystal (~1100 nm) is almost 100%, which indicates the absence of significant light scattering by QD agglomerates. Fig. 1b shows a transmission electron microscope (TEM) image demonstrating a QD monolayer without the formation of three-dimensional agglomerates. Fig. 1c shows an infrared (IR) absorption spectrum of SiQD 1100 stored in methanol for 60 days. An absorption peak at ~1080 cm^{-1} assigned to Si–O–Si stretching vibrations can be clearly observed while no

absorption peak is evident from C–H$_x$ (~2900 cm^{-1}). This suggests that following long-term storage in methanol, the surface of SiQDs is terminated principally by oxygen. After around one month's storage in methanol, the photoluminescence (PL) spectra of SiQD 1050 and 1100 under excitation at 450 nm exhibit PL peaks of around 750 and 850 nm respectively (Fig. 1d). The size-dependence of the PL peak wavelength of B and P co-doped Si QDs has already been studied in detail.[25]

With respect to the imaging of SiQD in cell cultures by means of fluorescence microscopy (wide-field or confocal), the presence of so-called autofluorescence (AF) – *i.e.* the natural fluorescence of cell proteins and other molecules without artificial staining must be considered. AF usually peaks in green but extends far into the red spectral region in which it overlaps with the PL of the tested SiQDs. This is illustrated in Fig. 2 which shows the local PL spectra of the AF and PL of SiQD 1100 under excitation by means of a laser at 405 nm. In general, three measures can be applied so as to improve the ratio of SiQD PL *versus* AF:

(i) The shifting of the excitation wavelength into the green region (*e.g.* the Ar-ion laser line at 488 nm) since AF decreases faster with red-shift excitation than does SiQD PL.

(ii) The selection of SiQDs with an emission peaking at long wavelengths where AF disappears but where microscope detectors remain efficient; this usually means between 700 and 800 nm.

(iii) The use of different PL decay kinetics under pulsed excitation. While AF decays within a few nanoseconds, SiQDs have a lifetime in the order of tens of microseconds. Therefore, gated detection can be applied which is delayed following pulsed excitation by around 5 ns. Fig. 3a shows the slow rate of PL decay for both the SiQD samples and Fig. 3b illustrates that PL decay under excitation by sub-ns pulse with high repetition rate (20 MHz – such a degree of excitation is deliverable by a large number of currently available confocal microscopes) was unable to follow the pulse sequence and thus quasi-constant PL was detected – the yellow rectangle indicates the temporal position of the detection gate (delay 5–12 ns) as used later in this paper (such excitation and detection options are available in a large number of the current models of confocal microscopes).

Finally, we draw attention to the aging of the luminescence properties of SiQDs. During long-term storage (around 1 year) a slow change in the PL peak position and the external quantum yield (EQY) can be observed in methanol suspensions of SiQDs, which is further accelerated in water-based suspensions used in bio-studies. Both types of SiQD exhibit a blue-shift and the EQY changes as illustrated in Fig. 2c roughly following a curve which has a maximum EQY of 12% for a peak at 750 nm (similar optimal conditions were reported by Liu *et al.*).[26] Such optimum conditions for fluorescence imaging are characteristic of fresh SiQD 1050 samples; however, upon aging such samples degrade in terms of EQY while SiQD 1100 shifts to the optimum position (a shift from 850 nm to 750 nm). In brief, it is essential that aging properties are characterized in order to be able to anticipate PL evolution and select the ideal sample.
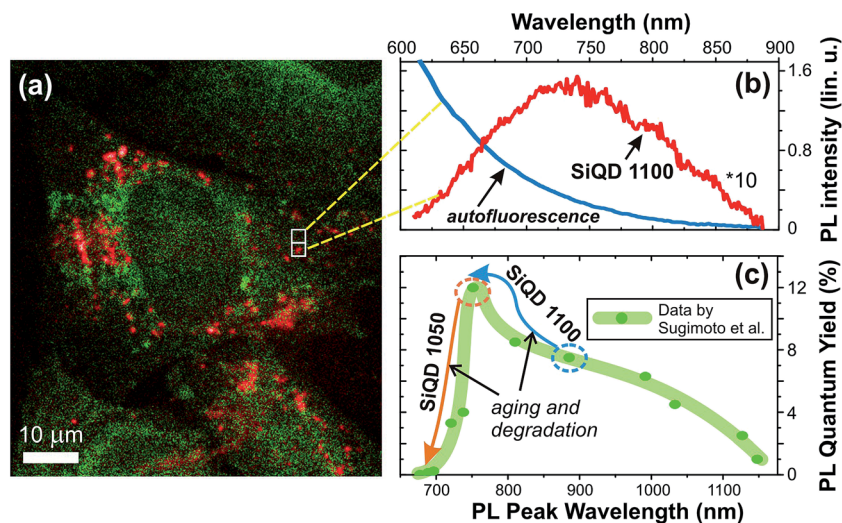
Fig. 2 Wide-field fluorescence microscopy and spectroscopy under cw excitation at 405 nm: (a) combined fluorescence image with the green layer showing the full signal (dominated by cell autofluorescence) and the orange layer showing signal above 785 nm (dominated by SiQD luminescence). The vertical stripe shows area of the spectrometer slit introduced for spectral measurements. (b) Luminescence spectrum of cell autofluorescence (blue) and emission of SiQD cluster (red line) from area indicated by a rectangle in the panel (a). The autofluorescence signal estimated from area around the SiQD cluster was subtracted and spectral shape corrected to the sensitivity of the experimental apparatus. The peak is around 730 nm. (c) Observed shift of PL peak and quantum yield of SiQDs with time is plotted together with data from the paper by Sugimoto et al.[20] The slow changes due to aging of SiQD suspensions in methanol are accelerated in water based media during bio-studies. The data (green line and points) on PL QY dependence on PL peak position (size of QDs) explains well why SiQD 1100 sample is well observed in cell cultures while luminescence of SiQD 1050 vanishes.

3.2 Zeta potential assessment

The zeta potential (ζ) of water suspensions of SiQD 1050 and 1100 as a function of pH was determined using 0.25 M NaOH, 0.2 M HCl and 0.02 HCl titration agents. The SiQDs had been titrated in the acid → base and base → acid direction (Fig. 4). The iso-electric point of both samples was determined at around pH 2. While SiQD 1100 reacted relatively smoothly to changes in pH, the SiQD 1050 reaction to the addition of acid/ base was slow and followed by sudden jumps in ζ. Moreover, a two-peak distribution of ζ was observed for SiQD 1050 at each pH point (Fig. 4d) indicating the presence of distinct SiQD fractions. For a pH of 7.5 (the value relevant to biological experiments) the mean value of ζ was around – 64 mV (−16 mV for the smaller peak) for SiQD 1050 and – 57 mV for SiQD 1100 (with an uncertainty of around 8 mV).

3.3 The effect of different SiQD concentrations on cell metabolic activity in serum-supplemented and serum-free media

Osteoblastic cells were cultivated in a medium supplemented with 5% fetal bovine serum (5% FBS-medium) with gradually increasing concentrations (25, 50 and 125 μg ml^{-1}) of two types of SiQD which was followed by the determination of their metabolic activity after 6, 24 and 48 hours (Fig. 5a and b). It is apparent that SiQD 1100 in a fully-supplemented medium had no impact on cell metabolic activity irrespective of concentration at the 6 hour time point; however, after 24 hours the highest concentration of SiQD 1100 decreased cell activity significantly and, after 48 hours, the medium concentration was seen to have a similar effect.

On the other hand, SiQD 1050 (lowest and medium concentrations) surprisingly increased cell metabolic activity after 6 hours and, after 24 hours of incubation, the metabolic activity of SiQD 1050-treated cells was comparable to that of controls with no treatment. Only after 48 hours did the highest concentration of SiQD 1050 significantly decrease cell metabolic activity.

In order to distinguish between the effect of SiQDs and the role of the protein corona (originating from serum proteins), osteoblastic cells were cultivated in a medium containing no supplements (serum free – 0% FBS-medium). The same concentrations of SiQDs were then added and the same tests performed as described above (under standard conditions). It is apparent (Fig. 5c and d) that the serum-free medium only (with no SiQDs) had a negative effect on cell metabolic activity at the 6 hour time point; however, the decrease was not so strong as to be considered cytotoxic.[27]

Those cells treated in the serum-free medium with the lowest and medium concentrations of SiQD 1100 exhibited a metabolic activity level similar to the control sample (cells cultivated in a 5% FBS-medium) and only in the highest SiQD concentration did cell activity decrease significantly to the cytotoxic level after 6 hours (in contrast to standard conditions). Subsequently, after 24 hours, both the medium and the highest concentrations of SiQD 1100 were found to strongly affect cell activity and, finally (after 48 hours) all the tested concentrations of SiQD 1100 in the serum-free medium were determined as being cytotoxic.

On the other hand, SiQD 1050 did not affect cell behavior at any concentration after 6 hours; however, after 24 hours of incubation, all the tested concentrations were found to be
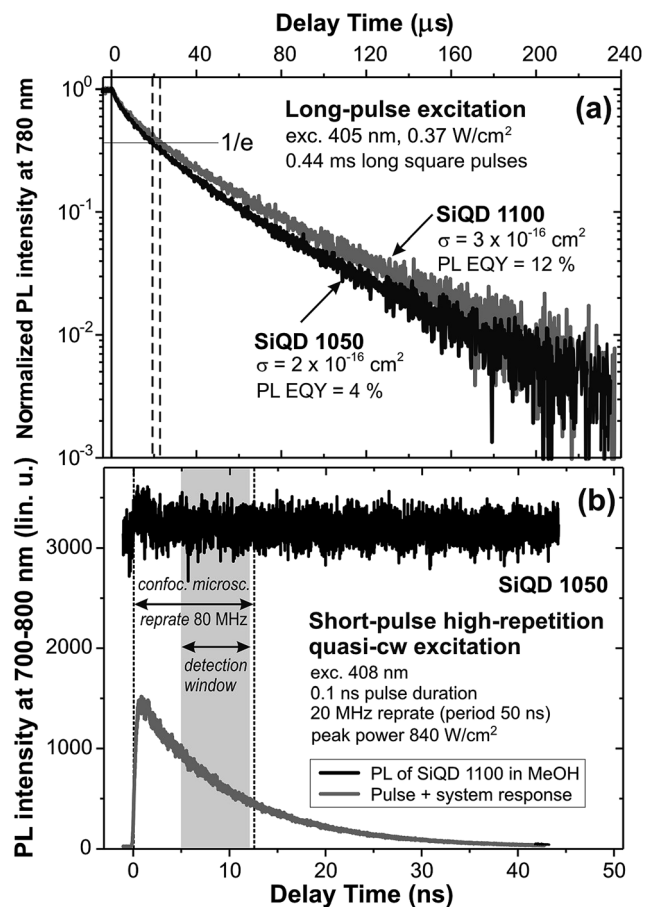
Fig. 3 (a) Kinetics of PL decay under long square pulses and (b) short high-repetition rate (quasi-cw) excitation. The conditions applied in the confocal imaging (80 MHz repetition rate, detection window of 7 ns delayed by 5 ns) is indicated by the yellow rectangle.

cytotoxic, the level of which was further enhanced following 48 hours of incubation.

3.4 The microscopy assessment of SiQD effects on cell morphology and metabolic activity in serum-supplemented and serum-free media

Osteoblasts were treated with 50 μg ml^{-1} of SiQD 1050 and SiQD 1100 (medium concentration) in a 5% FBS-medium for 2, 6 and 24 hours and then visualized by means of wide-field fluorescence microscopy accompanied by a phase contrast for the more precise localization of the SiQD fluorescence signal within the cells (Fig. 6a and b). Confocal microscopy images of cells treated with the same SiQD concentrations were acquired at the 24 hour time point only (Fig. 6c and d).

Fig. 6a shows that a very bright fluorescence signal is visible in those cells treated with SiQD 1100 as soon as after 2 hours and that it is even stronger at the 6 hour time point. However, it is apparent from the phase contrast image that the signal originates from a culture medium in which aggregates of SiQD with proteins originating within the FBS had formed and not from the cells themselves. After 24 hours, the fluorescence signal of SiQD 1100 is apparent from inside the cells as well as

from the culture medium itself. The confocal image (Fig. 6c) taken at the same time confirms the localization of these SiQDs inside cells in a vesicular form with no apparent changes in cell morphology. In addition, cell metabolic activity tests (Fig. 8a) indicated that these SiQDs had no negative impact on the cells at the same time point; only after 48 hours of incubation did the SiQD 1100 cause a significant decrease in cell metabolic activity but not to such an extent as to include cytotoxic effects.[27]

In the case of SiQD 1050 an even stronger fluorescence signal of SiQD and proteins in the cultivation medium was detected after 6 hours but only a very weak signal could be detected in the cells after 24 hours (Fig. 6b). The image of cells treated with SiQD 1050 for 24 hours presented was intentionally selected so as to show the cells in the region not totally covered with SiQD-protein aggregates; notwithstanding, most of the sample area was found to be covered with these foggy aggregates. This observation was confirmed by means of confocal imaging (Fig. 6d) which revealed a weak fluorescence signal distributed diffusely within the cells (autofluorescence) and a concentrated signal issuing from the culture medium in which SiQD 1050 aggregates and FBS proteins were formed. Indeed, this corresponds well with the data presented in Fig. 8b according to which no reduction in metabolic activity (compared to the untreated control in the 5% FBS-medium) was detected in either evaluation using the same concentration of SiQD 1050.

Subsequently, the same experiments were performed with using the serum-free medium (0% FBS-medium). Fig. 7a shows that a fluorescence signal is visible in those cells treated with SiQD 1100 as soon as after 2 hours of incubation and it is even stronger at the 6 hour point at which all the cells exhibit a fluorescence signal. After 24 hours, SiQD and protein aggregates were visible in the medium. The proteins originated from the FBS added to the culture medium after 6 hours due to the cells being unable to survive (*i.e.* to avoid significant behavioral changes) any longer without the addition of FBS. It was expected that all the SiQDs would already have entered the cells by this time point and that they would no longer be present in the medium. However, microscope images demonstrate that after 6 hours a certain amount of SiQD 1100 was still present in the medium available to react with the FBS proteins. Nevertheless, SiQD 1100 were present on a massive scale inside the cells at 24 hours (Fig. 7a) and had a negative impact on cell morphology; moreover, this led to a significant decrease in cell metabolic activity (Fig. 8a). The confocal image (Fig. 7c) confirms the presence of high quantities of SiQD 1100 inside the cells in the diffused form which is in contrast to the localization of SiQD 1100 in those cells cultivated in the 5% FBS-medium (Fig. 6c). Results concerning metabolic activity indicate that the cells were dying at a rapid rate at the 24 hour point and had died at the 48 hour time point.

Conversely, SiQD 1050 were practically invisible at all time points in those cells cultivated in the serum-free medium; a very faint signal was detectable at the 2 hour time point which disappeared over time (Fig. 7b). The wide-field microscopy data was confirmed by the confocal images in which the fluorescence signal was very faint and originated from cell autofluorescence. However, the results presented in Fig. 8b suggest that
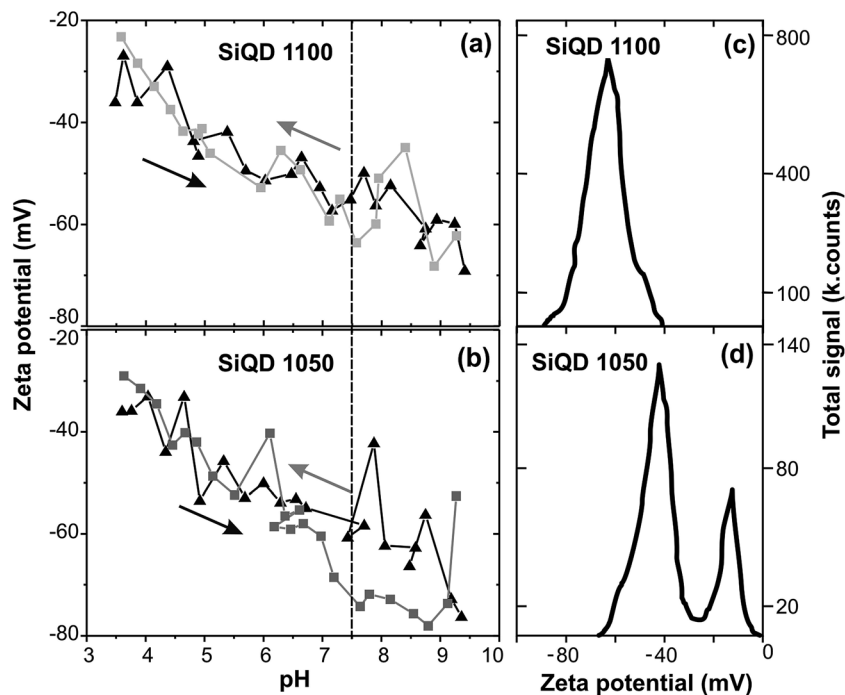
Fig. 4 Zeta-potential evaluation: (a) titration curves of SiQD 1100 and (b) SiQD 1050 (each point is average of three measurements). Small graphs show an example of single measurement of zeta potential at pH 7.5 in (c) SiQD 1100 and (d) SiQD 1050.

a reduction in metabolic activity occurred after 24 hours of incubation (also apparent in the form of changed cell morphology in Fig. 7b) and that at the 48 hour point the cells had already died.

This report presents the first study performed on the impact of novel Si-based nanoparticles on a biological environment consisting of a human osteoblast cell culture. The most unique property of the B and P co-doped SiQDs used consists of their
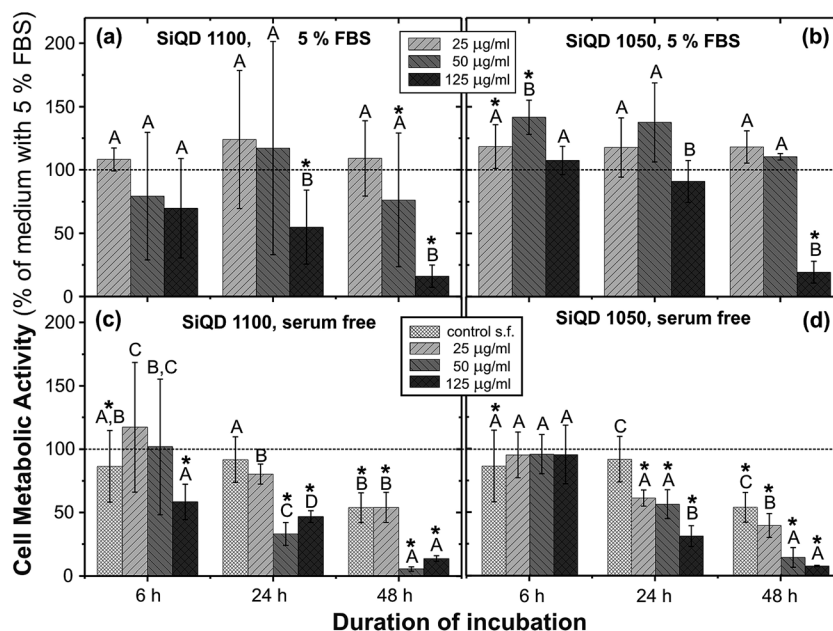

Fig. 5 Metabolic activity of osteoblasts cultivated in a cultivation medium supplemented with 5% FBS (a, b) and in serum free medium (c, d) for increasing concentration of SiQD 1100 (a, c) and SiQD 1050 (b, d). Relative values are expressed as a percentage of control sample in the cultivation medium with 5% FBS (dashed line). The star symbol (*) highlights a significant difference from the control in cultivation medium with 5% FBS (Wilcoxon matched-pairs test, $p < 0.05$). Groups marked with different letters express significant inter-group differences within time points (ANOVA, LSD *post hoc* test, $p < 0.05$).
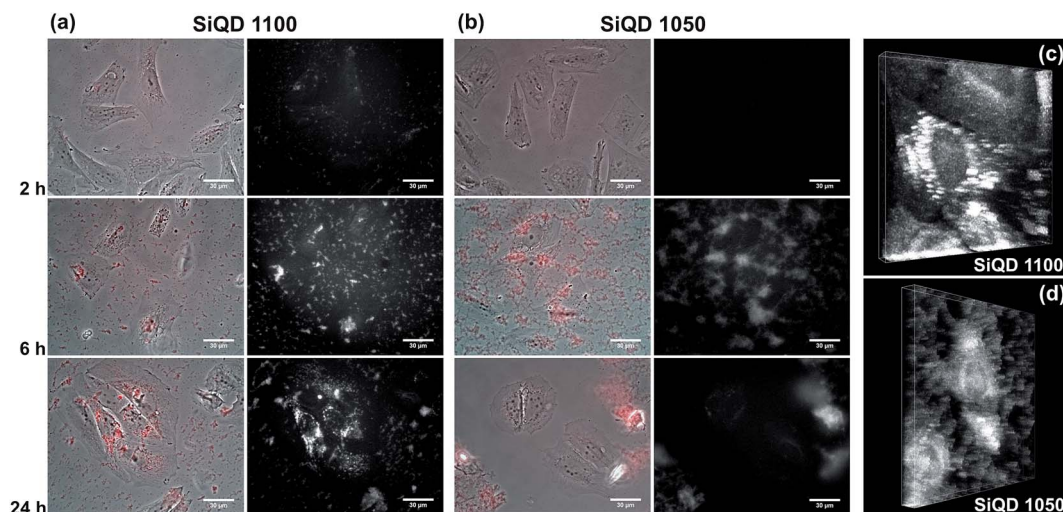
Fig. 6 Wide-field fluorescence and phase contrast microscope images of osteoblasts treated with (a) SiQD 1100 and (b) SiQD 1050 in 5% FBS-supplemented medium in different time points (the scale bar is 30 μm) and confocal images after 24 h of incubation with (c) SiQD 1100 (imaged volume 75.0 × 75.0 × 7.6 μm) and (d) SiQD 1050 (imaged volume 112.6 × 112.6 × 9.5 μm).

ability to form stable colloidal suspensions in the absence of surfactants and organic passivation. Moreover, these SiQDs required no protective shell layer and were of a very small size (3–4 nm in diameter) in contrast with other semiconductor quantum dots with a core–shell structure and which are substantially larger than 10 nm (not taking into account possible surface passivation) in order that they exhibit a stable emission in a similar spectral region on the border of red and infrared (700–850 nm).[28] We selected two types of SiQDs with sizes of 3 and 4 nm (SiQD 1050 and 1100 respectively) the PL emission peaks of which are situated in the afore-mentioned spectral range which is optimal in terms of fluorescence microscopy. Somewhat surprisingly, our experiments revealed significant differences with respect to the interaction of the two types of SiQD with cell cultures which could not be ascribed simply to the 1 nm size difference – at the cellular level such a small difference does not influence particle cytotoxicity and only a slight change in cellular uptake is able to occur.[29–31]

Zeta-potential (ζ) is related to colloidal suspension stability. The critical value of ζ below which a suspension is unstable (and at which agglomeration can take place) is around ±30 mV.[32] Generally, ζ is result of the net electrical charge contained within the region bounded by the slipping plane. This charge is strongly dependent on ions present in the solution and therefore changes with pH value. The pH value, for which the net electrical charge is null, is called isoelectric point. Around this point the nanoparticles aggregate rapidly. With concern to biology, the surface potential of a particle is important in terms of the formation of protein corona – nanoparticles with different potentials will bind to different proteins or to different active sites on individual proteins which, in turn, may significantly influence the overall toxicity of nanomaterials. An example of the varying degree of toxicity of Si nanoparticles depending on the value of ζ and the particle covering is reported in;[10,11] however, this effect has also been observed with respect

to other types of nanoparticles.[33,34] Our experiments resulted in different values of ζ for Si QD 1050 and 1100; therefore we suspect the formation of a differing protein corona under the same biological conditions.

Both of the tested SiQDs caused harm to the cells in a different manner – SiQD 1100 exhibited a measurable harmful effect at the highest applied concentration level (125 μg ml^{-1}) as soon as after 24 hours of incubation in the fully-supplemented medium, while the negative effect of SiQD 1050 was not apparent until after 48 hours of incubation (Fig. 5). It is conjectured that this difference may be linked to the observed formation of dense clusters of SiQD 1050 with serum proteins (see the fluorescence images in Fig. 6). These clusters act as reaction centers and continue to grow thus forming huge aggregates which cover the outside membranes of the cells and prevent SiQD 1050 from entering the cells. When subjected to fluorescence microscopy, protein/SiQD 1050 aggregates are visible as fog-like structures which grow over time (Fig. 6b and d). Despite this effect, however, a number of uncovered locations were detected after 48 hours thus providing coarse information on the incorporation of SiQD 1050 into the cells (Fig. 6b). This phenomenon was also witnessed with respect to SiQD 1100 but to a significantly lesser extent which, nevertheless, still allowed for the visualization of the cells and their incorporation of SiQD 1100. Notably, literature describes this aggregation effect with respect to other types of nanoparticles.[35,36] Therefore, it is safe to conclude that the presence of FBS proteins in the cultivation medium strongly influence specific SiQD behavior and thus their availability and absorption by cells. It may be speculated from the fluorescence images (Fig. 6c) that the SiQD 1100 visible in cell cytoplasm are localized in vesicles and thus potentially enter cells by means of endocytosis as has been previously described.[37–40]

When SiQDs were incubated with cells in the serum-free medium, SiQD 1100 exhibited a cytotoxic effect at the highest
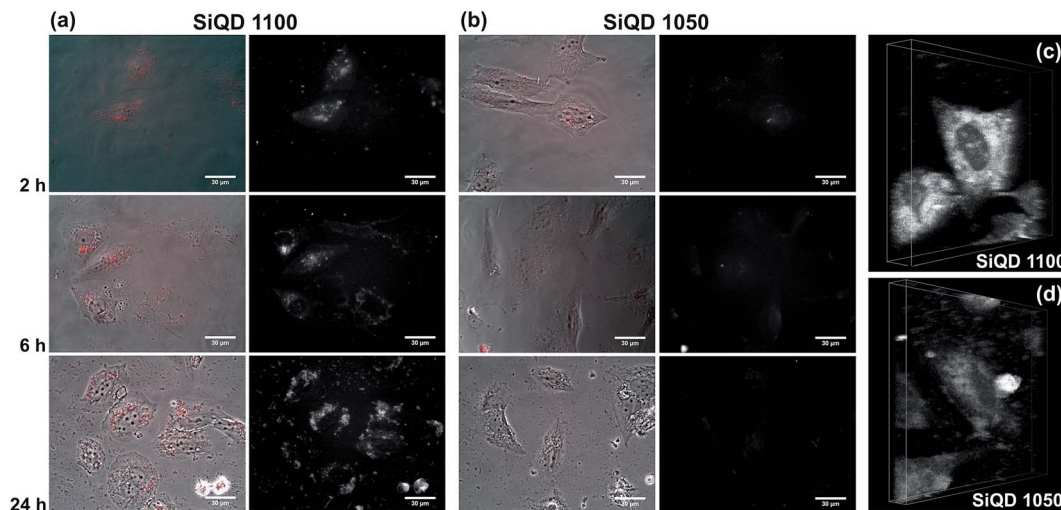
Fig. 7 Wide-field fluorescence and phase contrast microscope images of osteoblasts treated with (a) SiQD 1100 and (b) SiQD 1050 in the serum-free medium in different time points (the scale bar is 30 μm) and confocal images after 24 h of incubation with (c) SiQD 1100 (imaged volume 85.0 × 85.0 × 11.6 μm) and (d) SiQD 1050 (imaged volume 102.0 × 102.0 × 9.6 μm). Note – after 6 h of cell incubation in serum-free medium, FBS was added due to the cell survival purposes.
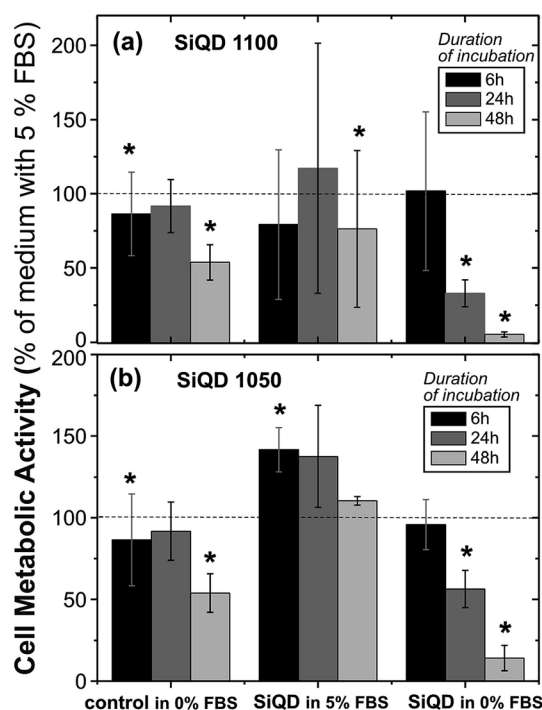

Fig. 8 Metabolic activity of osteoblasts treated with 50 μg ml^{-1} of (a) SiQD 1100 and (b) SiQD 1050 for different time points.

applied concentration level (125 μg ml^{-1}) as soon as after 6 hours of incubation (Fig. 5c). Therefore, it was concluded that bare SiQDs (without a protein corona) are able to cross cell membranes more easily and efficiently than treated SiQDs. This statement was subsequently proven by means of fluorescence imaging (Fig. 7a) which revealed the presence of SiQD 1100 in the cell cytoplasm but, surprisingly, that it was localized diffusely rather than in the form of whole spots as in the case of

standard cultivation conditions with the presence of FBS. It would appear that the way in which SiQD 1100 enter cells varies under different conditions (with or without a protein corona), a fact that might be studied in greater detail in the future. SiQD 1050 required a longer incubation time (24 hours) before they entered the cells under serum-free conditions; importantly, however, the effect was significantly stronger – all the concentrations of SiQD 1050 tested were found to be cytotoxic after 24 hours (Fig. 5d). Both SiQDs in the serum-free medium were seen to harm the cells earlier and at a lower concentration than under fully-supplemented medium conditions. It has already been mentioned that nanoparticles lower their surface free energy *via* strong non-specific interaction with cell membranes. However, the amount of free energy is lowered by the presence of a protein corona and both the degree of adhesion to the membrane and cell uptake are reduced.[41,42] Thus the observed effect of proteins bound to SiQDs inducing a delay in the onset of cytotoxic effects is not surprising and is in agreement with previous observations.[43,44]

SiQD 1100 were detected within the cells under both test conditions – both with and without proteins originating from FBS; however, it was found that without proteins they enter the cells more rapidly, are distributed diffusely and have a stronger negative effect on metabolic activity. On the other hand, SiQD 1050 were not detected in the cells by means of fluorescence microscopy under either of the test conditions; however, the cytotoxic effect thereof was determined (Fig. 8b) which may indicate their entry into the cells. Moreover, the cytotoxic effect was found to be stronger under non-FBS protein presence conditions. This may imply the easier cell entry of SiQD 1050 without a protein corona. However, they were not observable *via* fluorescence microscopy images. We suspect, as PL aging studies suggest (Fig. 2c), that the PL of these SiQDs degrades to a significant extent in aqueous media (*i.e.* in the natural biological experiment environment). Moreover, it should be noted

that SiQD 1050 exhibit three times lower PL EQY and a slightly lower absorption cross-section, which renders them more difficult to observe by means of fluorescence microscopy (Fig. 6b and d).

The formation and structure of the protein corona is crucial in terms of the fate of all nanoparticles located in living organisms as has been demonstrated by a large number of previous studies.[13,35,36,45] Bare nanoparticles are unable to survive within a biological system since they are immediately covered by a layer of proteins from the fluid which forms the hard protein corona and which continues to grow until they attain a stable state, which is often a long-term process as observed in the case of SiQD 1050. Experiments conducted prior to *in vivo* application should always mimic the environment of the organism as precisely as possible. *In vitro* dose-dependent tests of nanoparticles should be performed using biological fluids only before forming conclusions on the cytotoxicity of the material. As was apparent especially in the case of SiQD 1050, the presence of bare SiQDs or protein-coated SiQDs in the cell culture makes a huge difference in terms of cytotoxicity and the immense aggregation of SiQD 1050 with proteins leads to fatal consequences for organisms.

4 Conclusion

We attempted to demonstrate to what extent novel co-doped SiQDs react upon being introduced into a natural biological environment consisting of human osteoblasts and a cell culture medium with or without the addition of fetal bovine serum. A series of experiments was conducted at various concentration levels of two types of SiQD (1100 and 1050), an evaluation was made of their cytotoxicity and their localization within the cell culture was assessed by means of fluorescence wide-field and confocal microscopy.

The detailed luminescence characterization of the SiQDs in colloidal suspensions at different times following fabrication as well as of the SiQDs inside cell cultures and water-based media enabled the research team to uncover the continuous changes which took place due to the aging of the SiQDs (a shift in the PL peak to shorter wavelengths and related EQY changes, Fig. 2). A detailed knowledge of PL aging allowed us to select the optimum type of SiQD (*i.e.* SiQD 1100) for fluorescence imaging purposes in cells with an optimal PL peak of around 750 nm and an ensemble EQY of 12%.

Zeta potential measurement indicated that the tested SiQDs differ from each other not only in terms of their size and PL properties but also with respect to zeta potential values. Consequently, the formation of a protein corona differs on the surface of SiQDs, which affects the reaction with the biological components of the cell culture medium and overall cytotoxicity. SiQD 1050 in particular were almost completely entrapped within growing aggregates of proteins which hindered their access into the cells which, in turn, led to the cytotoxicity of SiQD 1050 appearing to be relatively low. However, the real extent of cytotoxicity was revealed under serum-free conditions indicating that a high amount of SiQD 1050 enter cells despite the fact that they become undetectable by fluorescence

microscopes (due to a PL shift to shorter wavelengths with strong cell autofluorescence and the degradation of PL yield). On the other hand, SiQD 1100 exhibited a low level of interaction with proteins which enabled cell incorporation even in the serum-supplemented medium. Thus, these particles are able to enter cells in the bare state as well as with the addition of a protein corona although in each case the pathways most probably differ.

The results provide important findings concerning the *in vitro* toxicity of novel co-doped SiQDs and enhance our understanding of the complexity of processes acting between SiQDs and biological environments.

Acknowledgements

References

1 K. K. Qian and H. R. Bogner, *J. Pharm. Sci.*, 2012, **101**, 444–463.

2 E. J. Anglin, M. P. Schwartz, V. P. Ng, L. A. Perelman and M. J. Sailor, *Langmuir*, 2004, **20**, 11264–11269.

3 F. Erogbogbo, K.-T. Yong, I. Roy, G. Xu, P. N. Prasad and M. T. Swihart, *ACS Nano*, 2008, **2**, 873–878.

4 Y. Zhong, X. Sun, S. Wang, F. Peng, F. Bao, Y. Su, Y. Li, S.-T. Lee and Y. He, *ACS Nano*, 2015, **9**, 5958–5967.

5 X. Pi, T. Yu and D. Yang, *Part. Part. Syst. Charact.*, 2014, **31**, 751–756.

6 S. E. A. Gratton, P. A. Ropp, P. D. Pohlhaus, J. C. Luft, V. J. Madden, M. E. Napier and J. M. DeSimone, *Proc. Natl. Acad. Sci. U. S. A.*, 2008, **105**, 11613–11618.

7 X. Yang, J. Liu, H. He, L. Zhou, C. Gong, X. Wang, L. Yang, J. Yuan, H. Huang and L. He, *Part. Fibre Toxicol.*, 2010, **7**, 1–12.

8 H. Liang, C. Jin, Y. Tang, F. Wang, C. Ma and Y. Yang, *J. Appl. Toxicol.*, 2014, **34**, 367–372.

9 J. Kim, H. Kim and M. Kim, *Int. J. Nanomed.*, 2014, **9**, 235–241.

10 S. Bhattacharjee, L. H. J. de Haan, N. M. Evers, X. Jiang, A. T. M. Marcelis, H. Zuilhof, I. M. C. M. Rietjens and G. M. Alink, *Part. Fibre Toxicol.*, 2010, **7**, 25.

11 S. Bhattacharjee, I. M. C. M. Rietjens, M. P. Singh, T. M. Atkins, T. K. Purkait, Z. Xu, S. Regli, A. Shukaliak, R. J. Clark, B. S. Mitchell, G. M. Alink, A. T. M. Marcelis, M. J. Fink, J. G. C. Veinot, S. M. Kauzlarich and H. Zuilhof, *Nanoscale*, 2013, **5**, 4870–4883.

12 H. Herd, N. Daum, A. T. Jones, H. Huwer, H. Ghandehari and C.-M. Lehr, *ACS Nano*, 2013, **7**, 1961–1973.

13 M. Cui, R. Liu, Z. Deng, G. Ge, Y. Liu and L. Xie, *Nano Res.*, 2014, **7**, 345–352.

14 E. Roduner, *Chem. Soc. Rev.*, 2006, **35**, 583–592.

15 A. Lesniak, F. Fenaroli, M. P. Monopoli, C. Åberg, K. A. Dawson and A. Salvati, *ACS Nano*, 2012, **6**, 5845–5857.

16 M. P. Monopoli, C. Aberg, A. Salvati and K. A. Dawson, *Nat. Nanotechnol.*, 2012, **7**, 779–786.

17 M. Hadjidemetriou, Z. Al-Ahmady, M. Mazza, R. F. Collins, K. Dawson and K. Kostarelos, *ACS Nano*, 2015, **9**, 8142–8156.

18 H.-J. Eom and J. Choi, *Environ. Health Toxicol.*, 2011, **26**, e2011013.

19 S. W. Ha, J. A. Sikorski, M. N. Weitzmann and G. R. Beck, *Toxicol. In Vitro*, 2014, **28**, 354–364.

20 J. Kasper, M. I. Hermanns, C. Bantz, S. Utech, O. Koshkina, M. Maskos, C. Brochhausen, C. Pohl, S. Fuchs, R. E. Unger and C. James Kirkpatrick, *Eur. J. Pharm. Biopharm.*, 2013, **84**, 275–287.

21 M. Fukuda, M. Fujii, H. Sugimoto, K. Imakita and S. Hayashi, *Opt. Lett.*, 2011, **36**, 4026–4028.

22 H. Sugimoto, M. Fujii, K. Imakita, S. Hayashi and K. Akamatsu, *J. Phys. Chem. C*, 2012, **116**, 17969–17974.

23 J. Valenta, *Nanosci. Methods*, 2014, **3**, 11–27.

24 J. Valenta, M. Greben, Z. Remeš, S. Gutsch, D. Hiller and M. Zacharias, *Appl. Phys. Lett.*, 2016, **108**, 023102.

25 H. Sugimoto, M. Fujii, K. Imakita, S. Hayashi and K. Akamatsu, *J. Phys. Chem. C*, 2013, **117**, 11850–11857.

26 X. Liu, Y. Zhang, T. Yu, X. Qiao, R. Gresback, X. Pi and D. Yang, *Part. Part. Syst. Charact.*, 2016, **33**, 44–52.

27 E. Flahaut, M. C. Durrieu, M. Remy-Zolghadri, R. Bareille and C. Baquey, *Carbon*, 2006, **44**, 1093–1099.

28 E. Petryayeva, W. R. Algar and I. L. Medintz, *Appl. Spectrosc.*, 2013, **67**, 215–252.

29 R. G. Mendes, B. Koch, A. Bachmatiuk, A. A. El-Gendy, Y. Krupskaya, A. Springer, R. Klingeler, O. Schmidt, B. Büchner, S. Sanchez and M. H. Rümmeli, *Biochim. Biophys. Acta*, 2014, **1840**, 160–169.

30 S. Chen, C. Zhang, G. Jia, J. Duan, S. Wang and J. Zhang, *Mater. Sci. Eng., C*, 2014, **43**, 330–342.

31 W. Zhang, M. Kalive, D. G. Capco and Y. Chen, *Nanotechnology*, 2010, **21**, 355103.

32 D. Fennell Evans and H. Wennerström, *The Colloidal Domain: Where Physics, Chemistry, Biology, and Technology Meet*, Wiley, New York, 2nd edn, 1999.

33 A. Asati, S. Santra, C. Kaittanis and J. M. Perez, *ACS Nano*, 2010, **4**, 5321–5331.

34 A. M. El Badawy, R. G. Silva, B. Morris, K. G. Scheckel, M. T. Suidan and T. M. Tolaymat, *Environ. Sci. Technol.*, 2011, **45**, 283–287.

35 M. P. Calatayud, B. Sanz, V. Raffa, C. Riggio, M. R. Ibarra and G. F. Goya, *Biomaterials*, 2014, **35**, 6389–6399.

36 W. Jiang, K. Lai, Y. Wu and Z. Gu, *Arch. Pharmacal Res.*, 2013, **37**, 129–141.

37 L. W. Zhang and N. A. Monteiro-Riviere, *Toxicol. Sci.*, 2009, **110**, 138–155.

38 S. Ohta, S. Inasawa and Y. Yamaguchi, *Biomaterials*, 2012, **33**, 4639–4645.

39 A. Anas, T. Okuda, N. Kawashima, K. Nakayama, T. Itoh, M. Ishikawa and V. Biju, *ACS Nano*, 2009, **3**, 2419–2429.

40 P. Shen, S. Ohta, S. Inasawa and Y. Yamaguchi, *Chem. Commun.*, 2011, **47**, 8409–8411.

41 A. Lesniak, A. Salvati, M. J. Santos-Martinez, M. W. Radomski, K. A. Dawson and C. Åberg, *J. Am. Chem. Soc.*, 2013, **135**, 1438–1444.

42 P. Foroozandeh and A. A. Aziz, *Nanoscale Res. Lett.*, 2015, **10**, 221.

43 X. Jiang, S. Weise, M. Hafner, C. Röcker, F. Zhang, W. J. Parak and G. U. Nienhaus, *J. R. Soc., Interface*, 2010, **7**(1), S5–S13.

44 F. Catalano, L. Accomasso, G. Alberto, C. Gallina, S. Raimondo, S. Geuna, C. Giachino and G. Martra, *Small*, 2015, **11**, 2919–2928.

45 N. A. Monteiro-Riviere, M. E. Samberg, S. J. Oldenburg and J. E. Riviere, *Toxicol. Lett.*, 2013, **220**, 286–293.